Evaluation of Different Model Space Approaches Based on DFT to Examine the EPR Parameters of a Radiation-Induced Radical in Solid-State α-Glycine

Ewald Pauwels,* Veronique Van Speybroeck, and Michel Waroquier

Center for Molecular Modeling, Laboratory of Theoretical Physics, Ghent University, Proeftuinstraat 86, B-9000 Ghent, Belgium

Received: February 18, 2004; In Final Form: October 6, 2004

In this work, we present an extensive investigation of the radiation-induced $^{+}NH_3-{}^{\bullet}CH-CO_2^{-}$ glycine radical, using ab initio density functional modeling. The geometry and electron paramagnetic resonance (EPR) characteristics of the radical have been calculated using several model space approaches, including a single molecule approach, cluster models, and periodic calculations. Consecutively, both the calculated structural and spectroscopic properties are compared with experimental values taken from the literature. This comparative study involves the reproduction of the hyperfine coupling constants and the principal directions of the hyperfine tensor. It is found that the accurate calculation of these two features represents a sensitive probe for the accuracy of the proposed methodology to describe the glycine radical. The best overall agreement with experimental EPR parameters is found for a cluster calculation, in which the molecular environment surrounding the radical was explicitly taken into account, not only for the geometry optimization but also for the calculation of the spectroscopic properties. In the case of the $^{+}NH_3-{}^{\bullet}CH-CO_2^{-}$ glycine radical, apparently, the magnetic properties are indeed affected by the crystal environment.

1. Introduction

Due to the basic importance of amino acids and peptides in biochemistry, amino acid radicals have gained interest, not only in reactivity and radiation chemistry[1] but also in connection with radical proteins.[2] Ever since the first electron paramagnetic resonance (EPR) analyses of the radiation-induced radicals in solid-state α-glycine, the simplest amino acid, a vast amount of studies have appeared concerning their precise structure, from both an experimental and theoretical point of view.

In the mid-1950s already it was established that at least two radicals contribute to the EPR spectrum of irradiated glycine.[3,4] Ghosh and Whiffen[5] found one of these species to be a radical in its zwitterionic form, $^{+}NH_3-{}^{\bullet}CH-CO_2^{-}$, which was later confirmed in other studies.[6,7] The other major paramagnetic component was subject to some controversy,[3,8] but eventually the $^{\bullet}CH_2COOH$ structure was proposed.[9] Later on, several other (minor or transient) radicals were detected in the irradiated lattice.[10,11] Glycine radicals have also been reported in the liquid[12] and gas phases.[13] Only recently has an extensive review appeared on the solid-state radiation chemistry of glycine.[14]

In this work, we will concentrate on the $^{+}NH_3-{}^{\bullet}CH-CO_2^{-}$ radical in solid-state glycine as it is the major paramagnetic species formed at room temperature and because it closely resembles the zwitterionic glycine molecule in the solid state. Based on the work of Ghosh and Whiffen,[5] several other EPR analyses were performed on this radical. Hedberg and Ehrenberg[15] suggested some corrections for the proton hyperfine tensors, based on a spectral resolution enhancement technique. More recently, Sanderud and Sagstuen[16] made an elaborate study of irradiated glycine crystals, using EPR, electron nuclear double resonance (ENDOR), and ENDOR-induced EPR (EIE). They not only measured enhanced hyperfine tensors for the discussed radical but also detected three new paramagnetic species.

Prompted by the wealth of experimental results, several theoretical studies have been performed on glycine and its associated radicals.[17−20] Furthermore, the advent of density functional theory (DFT) has sparked a new impulse in the calculation of EPR parameters, as it cost-effectively incorporates electron correlation.[21,22] Nonetheless, for these calculated parameters to be in accordance with experiment, a decent radical conformation has to be obtained first and this is somewhat problematic with zwitterionic amino acids. High-level ab initio calculations have shown that the zwitterionic form of a single glycine molecule is not the energetically most favored structure in a vacuum. Instead, it undergoes intramolecular proton transfer from the amino group to one of the oxygen atoms to adopt the nonionic form.[17] Correspondingly, Barone et al. showed that the zwitterionic form for an isolated glycine radical does not correspond to a stationary point.[18] Therefore, to study glycine or one of its derived radicals in the solid state (or solution), it is essential to account for intermolecular environmental effects. Barone et al. addressed this problem by imposing constraints on a single glycine radical during optimization in a vacuum.[18] Others have kept the radical in its zwitterionic form by using a continuum model.[23] In these solvent simulation models, the radical under study is basically placed in a cavity surrounded by a continuum with a uniform dielectric constant. Within this methodology, Ban et al.[19] obtained the isotropic and anisotropic hyperfine couplings for all glycine radicals and compared these with experimental solid-state data. Using a conductor-like variant of the polarizable continuum model (CPCM), Rega et al.[20] calculated the vibrationally averaged isotropic hyperfine coupling constants for comparison with solution EPR couplings.

Despite the evident usefulness of these single molecule calculations, they mainly give information on the isotropic hyperfine coupling constants. The experimental data on the

* Corresponding author. Fax: 32 9 264 65 60. E-mail: ewald.pauwels@UGent.be.

10.1021/jp049251a CCC: $27.50
Published on Web 11/23/2004

principal axes of the hyperfine interaction tensor are nearly inaccessible for such a model space, but are still very valuable in a final comparative study between theory and the experimental signals. These three axes are experimentally determined by their corresponding direction cosines with respect to the reference frame, which usually coincides with the crystal axes. Within the single molecule approach, it is very tricky to insert the same reference axis system as was done in the experiment. To still do this, a crude approximation can be used to fix a priori both the orientation and part of the radical conformation. Although this method was used quite successfully in the case of the radiation-induced radicals of solid-state α-D-glucose,[24] it can be assumed that it is not commonly applicable. A more natural way to insert the reference frame is to explicitly include a part of the surrounding crystal lattice in the calculation. Cluster models offer this possibility, in which some intermolecular interactions are taken into account quite accurately, depending on the level of theory. These models, first introduced by Saebo et al.,[25] allow the optimization of a radical structure within a part of the solid state that is built up by several intact molecules around the defect, which have coordinates that are in accordance with crystal diffraction data. In a previous study by the authors, their feasibility and adequacy to describe crystal matrix effects, such as the formation of hydrogen bonds or displacements of atoms, was investigated for the radiation-induced radicals in the L-α-alanine crystal.[26] Another possibility to simulate the crystal lattice is by performing periodic calculations. In this method, the radical is properly embedded in its crystalline environment. By imposing periodic boundary conditions, boundary effects are eliminated, provided that the selected unitary cell containing the radical is large enough. In refs 26 and 27 we used a Car−Parrinello-based approach[28] on the R2 radical of alanine and on the glycine radical. In this work, the stable structures of the radical are found by a similar approach in which the electronic and nuclear degrees of freedom are optimized simultaneously.

As recently stressed in a review by Improta and Barone,[29] several effects have to be considered when calculating EPR properties of organic radicals. In addition to the influence of the level of theory on the optimized radical geometry, environmental and even dynamical effects can be taken into account. The latter are important for a good reproduction of hyperfine coupling constants, especially for flexible (nonrigid) paramagnetic systems such as radicals in solution. The environment of the radical also has considerable influence on the spectroscopic properties, and accounting for these effects is quite important when dealing with the dense structure of a crystal matrix.

Since the impact of vibrational averaging effects was already carefully studied by Barone et al.[18] and Rega et al.,[20] we have concentrated in the present article on the influence of environmental effects on the $^{+}NH_3-{}^{\bullet}CH-CO_2^{-}$ radical in solid-state glycine. For this purpose, the three aforementioned methodologies have been used. In a first attempt, the radical defect in glycine is modeled using an adapted single molecule approach, as described in ref 24. In the second approach, high-level DFT cluster models are employed to obtain a valid conformation of the radical. In the third approach, ab initio periodic calculations are performed. The results of all these optimizations are then used to calculate the EPR parameters for the different conformations. To also examine the influence of the neighboring lattice on the electronic structure of the central radical, EPR calculations were performed both on the single radical and on the radical in its cluster environment. During the subsequent analysis of the spectroscopic properties, special attention is paid to the reproduction of the calculated principal axes of the hyperfine tensor. It is shown that a reliable investigation of these principal axes offers an extra tool to improve the structural modeling of organic radicals in the solid state.

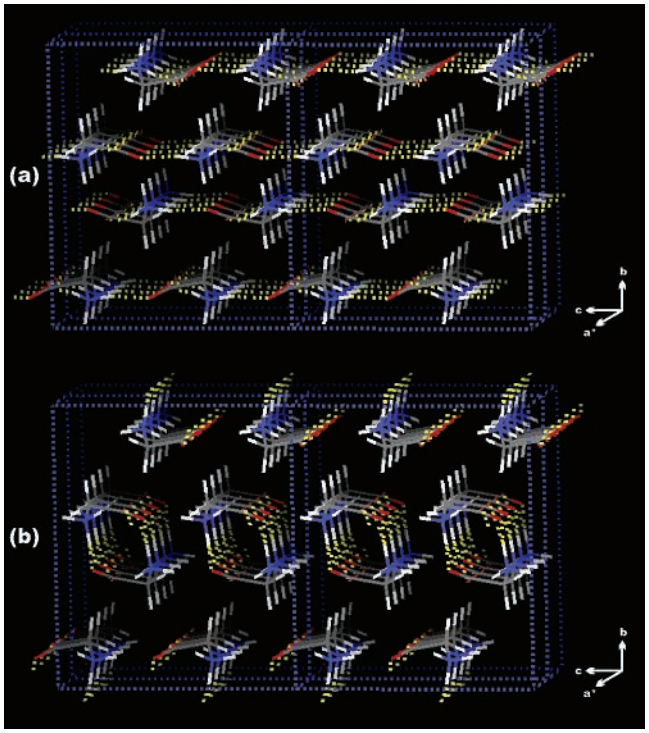

Figure 1. Four enlarged unit cells (with the original unit cell doubled in the a and c directions), illustrating the hydrogen bonding scheme in solid-state α-glycine. (a) Layers of glycine molecules are formed within the crystal by short hydrogen bonds (interactions a and c). (b) One long hydrogen bond and a short van der Waals contact hold together adjacent layers (interactions b and d, respectively).

The paper is organized as follows. After some theoretical considerations and the computational details (section 2), we will first evaluate the value of the cluster and periodic approaches to describe intermolecular interactions in solid-state glycine (section 3). Subsequently, the different optimized radical geometries will be examined and compared with the original crystal structure (section 4). In section 5, the calculated EPR parameters are analyzed and compared with experimental data. Finally, some general conclusions are made.

2. Theoretical Considerations and Computational Details

The α-glycine crystal reveals space group symmetry $P2_1/n$ and has four glycine molecules in the monoclinic unit cell. In what follows, we refer to the atomic lattice coordinates of a recent X-ray diffraction study at 23 K[30] where also the unit cell constants were determined as $a = 5.087$ Å, $b = 11.773$ Å, $c = 5.460$ Å, and $\beta = 111.99°$ at the specified temperature. As is illustrated in Figure 1a, the glycine crystal structure can be best described as consisting of layers, perpendicular to the b axis, which are formed by two short hydrogen bonds ($O_4-H^a = H_6-O^a = 1.748$ Å and $O_5-H^c = H_7-O^c = 1.821$ Å). The atomic numbering is defined in Figure 2. Adjacent layers are held together by a slightly weaker hydrogen bond ($O_5-H^d = H_8-O^d = 2.04$ Å) and a short van der Waals contact ($O_4-H^b = H_8-O^b = 2.387$ Å), as shown in Figure 1b. Considering the last interaction to be an extremely weak hydrogen bond, an actual network of bifurcated hydrogen bonds mainly keeps the

TABLE 1: Overview of Selected Geometrical Features for Optimized Crystal Geometries, in Comparison with Experimental Crystal Structure Data, Taken from Ref 30[a]

		optimized crystal geometry						
		cluster approach		periodic approach				
	expt	B3LYP/PM3/7	B3LYP/7	BP86/PW/4	BP86/PW/16ab	BP86/PW/16ac	BP86/PW/16bc	BP86/PW/32
				Bond Lengths				
C1−C2	1.527	1.515	1.533	1.532	1.521	1.512	1.522	1.513
C1−O4	1.257	1.267	1.257	1.271	1.273	1.279	1.282	1.279
C1−O5	1.259	1.261	1.259	1.279	1.284	1.283	1.278	1.283
C2−N3	1.482	1.537	1.480	1.459	1.461	1.480	1.486	1.481
C2−H9	1.080/1.090	1.091/1.091	1.092/1.087	1.098/1.104	1.098/1.096	1.098/1.094	1.098/1.099	1.098/1.094
N3−H6	1.036	1.048	1.045	1.094	1.096	1.070	1.073	1.070
N3−H7	1.024	1.058	1.043	1.058	1.057	1.059	1.063	1.059
N3−H8	1.024	1.052	1.034	1.044	1.042	1.043	1.044	1.044
				Dihedral Angles				
O4−C1−C2−N3	19.5	29.1	22.2	24.3	37.6	22.9	15.0	22.8
O5−C1−C2−N3	−161.3	−149.5	−157.1	−157.0	−145.1	−158.1	−166.4	−158.3
H6−N3−C2−C1	177.3	177.9	176.0	168.7	177.2	175.8	175.5	175.9
H7−N3−C2−C1	−60.6	−57.5	−61.6	−71.4	−64.7	−62.0	−64.4	−62.0
H8−N3−C2−C1	57.9	55.9	59.0	49.3	55.6	56.9	55.7	56.8
				Improper Torsion Angles				
C2−O4−O5−C1	0.6	−1.0	−0.5	0.9	1.8	0.7	0.9	0.7
C1−N3−H9−C2	−37.5/36.0	−36.5/36.1	−36.7/35.9	−34.0/34.9	−35.2/34.2	−36.6/35.2	−35.7/35.3	−36.7/35.3
				Hydrogen Bonding Distances				
O4−Ha	1.748	1.730	1.738	1.498	1.527	1.718	1.714	1.718
O4−Hb	2.387	2.327	2.368	2.514	2.578	2.429	2.413	2.429
O5−Hc	1.821	1.760	1.733	1.733	1.729	1.742	1.790	1.746
O5−Hd	2.040	1.833	1.925	2.129	1.973	2.033	2.170	2.031
H6−Oa	1.748	1.747	1.706	1.498	1.527	1.703	1.669	1.706
H7−Oc	1.821	1.813	1.792	1.733	1.766	1.748	1.790	1.751
H8−Od	2.040	1.833	1.962	1.966	1.946	2.013	2.024	2.015
H8−Ob	2.387	2.439	2.283	2.401	2.421	2.352	2.336	2.355

[a] Units of bond lengths are angstroms. The atomic numbering scheme refers to that presented in Figure 2.

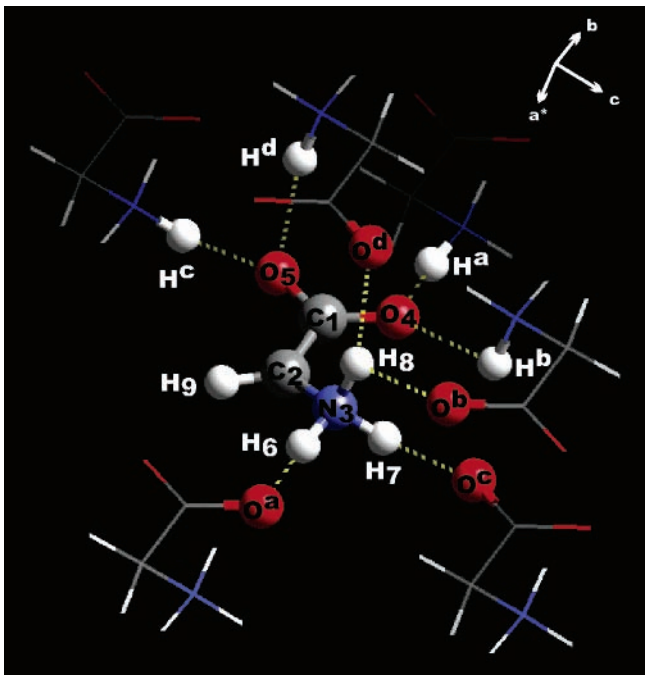

Figure 2. B3LYP/PM3/7 optimized geometry for the glycine radical, illustrating the model space in the cluster approach. Yellow dashed lines give an enhanced view of the hydrogen bonds presented in Figure 1.

glycine crystal structure together. These and other representative geometrical features are listed in the left column of Table 1.

2.1. Single-Molecule Approach. An initial geometry for the radical was obtained by removing a $-CH_2-$ hydrogen from the original glycine crystal structure to obtain a $^{+}NH_3-{}^{\bullet}CH-CO_2^{-}$ structure. Geometry optimization calculations were then performed on this radical structure within a "partial optimization" computational regime, outlined in detail in ref 24. Applied to glycine, this scheme essentially implies that only the C_2 and H_9 atoms were allowed to relax, while all other atoms were kept fixed at their original position in the crystal structure during optimization. Evidently, this is an artificial choice and other constraints could be imposed, provided the radical geometry is restricted to maintain the zwitterionic structure. To allow for the determination of the hyperfine tensor principal directions later on, the partial geometry optimizations were performed using the NOSYMM keyword in the Gaussian03 software package.[31] This keyword constrains the software package not to shift or rotate the Cartesian coordinates of the radical model with respect to the reference frame and so a direct link with the original crystal axes is preserved.

The calculations were performed within a DFT framework,[32] employing the B3LYP functional,[33] since several studies[26,34,35] have indicated that this functional gives a reliable description of the geometry of a radical. Molecular orbitals were expanded in a triple-ζ 6-311G** basis augmented with single d and p polarization functions.[36] In what follows, we will refer to the results of these calculations with the B3LYP/1 shorthand.

2.2. Cluster Model. A cluster model of glycine molecules was constructed in accordance with the structure of the α-glycine crystal as determined from X-ray diffraction.[30] In this lattice, an initial cluster was obtained by considering all molecules that are engaged in hydrogen bonds with a central glycine molecule. As a result, a model space of seven molecules was obtained. A starting geometry for the radical $^{+}NH_3-{}^{\bullet}CH-CO_2^{-}$ was obtained by abstracting one $-CH_2-$ hydrogen atom from the central glycine molecule. This model is shown in Figure 2.

The radical structure was then fully optimized within the constrained cluster in search for conformations with minimal

energy. During these calculations, all "lattice" molecules surrounding the central defect were held fixed at their crystal positions. Initially, a layered ONIOM[37] approach of the system, as implemented in Gaussian03,[31] was adopted, since it proved quite successful and cost-effective in an earlier, analogous study on the radiation products of L-α-alanine.[26] In this ONIOM scheme, the central radical or "inner" layer is treated at a high level of theory (DFT-B3LYP with the 6-311G** basis set) while the surrounding glycine molecules, the "outer" layer, are described using a semiempirical PM3 Hamiltonian.[38] The optimized glycine radical conformation thus obtained will be referred to with the abbreviation B3LYP/PM3/7.

Subsequently, a second, larger cluster was also considered within this methodology, obtained by extending the original cluster of six with four additional lattice molecules, all having at least one atom closer than 4.0 Å from the center of mass of the central glycine radical. The resulting model space, thus consisting of one radical and nine surrounding molecules, was also subjected to the ONIOM optimization mentioned above, and the resulting conformation is referred to as B3LYP/PM3/10.

Additional calculations were performed on the small cluster, treating both glycine radical and lattice molecules at a full ab initio B3LYP level, with a 6-311G** basis. The results of these quite exhaustive calculations will be labeled B3LYP/7.

To assess the accuracy of the various models to describe the geometry of the glycine crystal, complementary calculations were performed on a small cluster of seven undamaged glycine molecules. Analogous to a similar study on L-α-alanine,[34] the optimization procedure presented above for the B3LYP/PM3/7 and B3LYP/7 approaches was reapplied on an intact central glycine molecule. The resulting geometrical parameters (which are given in Table 1) allow for a direct comparison with the experimentally determined conformation in the crystal lattice.

2.3. Periodic Calculations. To properly simulate the radical in the crystal lattice within a periodic approach, it is necessary to ensure that radical defects in adjacent unit cells are well separated from each other. This can be established by enlarging the unit cell and treating the resulting supercell in a periodic scheme. In a previous study on L-α-alanine[34] the crystal unit cell was doubled in the a and c directions. To verify whether such a model space is also valid for glycine, calculations were performed using different supercell sizes. In the BP86/PW/4 method, the supercell simply equals the unit cell. The BP86/PW/16ab, BP86/PW/16ac, and BP86/PW/16bc abbreviations refer to calculations in which the model space consists of sixteen glycine molecules, obtained by doubling the unit cell in the a and b, the a and c, and the b and c directions, respectively. Finally, periodic calculations were performed with an enlarged supercell containing 32 molecules, obtained by doubling the unit cell in the a, b, and c directions (BP86/PW/32abc).

The validity of these model space approaches was tested by performing geometry optimizations on the undamaged glycine crystal. A simulated annealing technique as proposed by Car and Parrinello[28] was applied in which the central molecule was allowed to relax, while the coordinates of all other atoms were kept fixed at their experimental geometries. The global minima at $T = 0$ K were localized with the aid of the CPMD molecular dynamics program,[39] by simultaneously optimizing the electronic and nuclear degrees of freedom. The electronic structure was described within the DFT formalism with use of the BP86 gradient corrected functional.[40] Very soft pseudopotentials of the Vanderbilt type were used to account for the core, with the use of an energy cutoff of 25 Ry (1Ry = 1314 kJ/mol) for the plane wave expansion.[41]

In a second set of calculations, the procedures presented above were applied to optimize the structure of a central radical within the various supercells.

2.4. EPR−DFT Calculations. We refer to standard works[22,42,43] for a detailed description of the theoretical EPR principles but summarize the most essential theoretical equations. The hyperfine coupling interaction, which is the most structure dependent EPR parameter for the discussed types of organic radicals, embodies the interaction between the electronic spin and nuclear spin magnetic moments. This interaction is included in the spin Hamiltonian, which holds all interactions taking place in the molecular system in the presence of a magnetic field. For a paramagnetic system characterized by an electronic spin $S = 1/2$ and nuclear angular moment $I = 1/2$, the general expression for this Hamiltonian can be simplified to

$$H = \beta_e \mathbf{B}\cdot\mathbf{g}\cdot\mathbf{S} - g_n\beta_n \mathbf{I}\cdot\mathbf{B} + \mathbf{S}\cdot\mathbf{A}\cdot\mathbf{I}$$

where β_e is the Bohr magneton, β_n is the nuclear magneton, and g_n is the nuclear magnetogyric ratio. The first two terms in the spin Hamiltonian reflect the electronic and nuclear Zeeman contributions and arise from the interaction of the external magnetic field **B** and the magnetic moments of the electrons and nuclei, specified by **S** and **I**, respectively. In the first Zeeman term, **g** represents the so-called g-tensor. The hyperfine interaction matrix **A** in the last term of the spin Hamiltonian is often divided into an isotropic and anisotropic part

$$\mathbf{A} = A_{iso}\mathbf{1} + \mathbf{T}$$

where **1** is the 3 × 3 unit matrix. The isotropic part A_{iso} of the hyperfine matrix (the hyperfine coupling constant or hfcc) arises from the coupling between the magnetic moments of the electrons *i* and the nucleus *n* through a contact interaction. It depends solely on the unpaired spin density $\sum_{\mu,\nu} P_{\mu,\nu}^{\alpha-\beta}$ at the position of the nucleus. This is shown in the following equation, assuming the g-tensor is isotropic

$$A_{iso}^{n} = \frac{8\pi}{3} g\beta_e g_n \beta_n \sum_{\mu,\nu} P_{\mu,\nu}^{\alpha-\beta} \langle \varphi_\mu(r_{ni}) | \delta(r_{ni}) | \varphi_\nu(r_{ni}) \rangle$$

where φ_μ and φ_ν are atomic orbitals centered on nucleus *n*. The anisotropic part of the hyperfine matrix is due to the interaction of magnetic dipoles, and is described by the following equation

$$T_{kl}^{n} = g\beta_e g_n \beta_n \sum_{\mu,\nu} P_{\mu,\nu}^{\alpha-\beta} \langle \varphi_\mu(r_{ni}) | r_{ni}^{-5} (r_{ni}^{2}\delta_{kl} - 3 r_{ni,k} r_{ni,l}) | \varphi_\nu(r_{ni}) \rangle$$

for the *kl*th component of the 3 × 3 anisotropic hyperfine interaction matrix **T**. Diagonalization of this matrix yields the three eigenvalues (or principal components) and corresponding eigenvectors (or principal axes) relative to the reference axis system.

In this study, the Gaussian03 software package was used to calculate isotropic and anisotropic hyperfine couplings, as well as the associated principal axes. This was done again using a B3LYP functional within the DFT framework. Even though specialized basis sets exist for EPR calculations (such as the EPR−III basis set of Barone[21]), we chose to perform all calculations in 6-311G**. Earlier studies by the authors[44] have

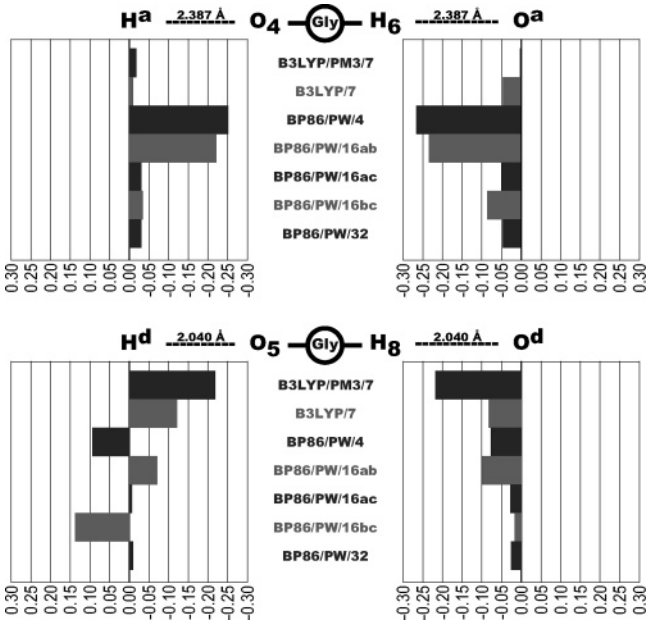

Figure 3. Schematic representation of relative differences between calculated and crystallographic hydrogen bond distances (in Å). Only the hydrogen bond interactions a and d are presented.

shown this level of theory to be sufficient for the calculation of EPR parameters in organic radicals.

For cluster or periodic lattice models, the EPR parameters were initially determined solely on the optimized structure of the central radical, without taking into account the neighbors. Hence, these are effectively single-molecule EPR calculations. To evaluate the influence of neighboring lattice molecules on the EPR parameters of the central radical and thus on its electronic structure, the paramagnetic properties were also calculated for the full cluster. The results of these calculations will be referred to with the additional label "(full)", as the complete model space was accounted for in the EPR calculation. Similar calculations within a periodic approach were, however, impossible as these are not yet implemented in the CPMD code.

3. Model Assessment for Cluster and Periodic Approach

The various models for describing the environmental forces on the geometry were tested by performing a comparative study between calculated and experimental geometrical data of the undamaged glycine crystal. The resulting structural features of the optimized geometries are given in Table 1.

The B3LYP/7, BP86/PW/16ac, and BP86/PW/32 levels of theory offer the best description of the glycine crystal. Bond lengths are described within 0.04 Å from the crystal structure and (improper) torsion angles within 5°. Hydrogen bond distances are perhaps the most sensitive and powerful indicators of the model approach performance to describe intermolecular interactions. Figure 3 schematically shows the relative differences between the calculated and crystallographic hydrogen bond distances for hydrogen bond interactions a and d. In the B3LYP/7 optimized geometry, all hydrogen bond lengths are slightly underestimated, with an acceptable maximum deviation of 0.1 Å. Hydrogen bond lengths are nearly identical for the BP86/PW/16ac and BP86/PW/32 geometries and are in slightly better agreement since the maximum deviation with the crystal structure is only 0.8 Å.

When part of the cluster is treated at the semiempirical level, substantially larger deviations are noticed for all geometrical features. The B3LYP/PM3/7 optimized central glycine molecule displays a particularly longer C_2-N_3 bond and its CO_2 group is rotated away from its original crystal structure orientation, as revealed by the dihedrals $O_4-C_1-C_2-N_3$ and $O_5-C_1-C_2-N_3$. The semiempirical B3LYP/PM3/7 approach also fails in predicting correct hydrogen bond interactions of type d: the O_5-H^d and H_8-O^d bond lengths are more than 0.2 Å underestimated. This is illustrated in Figure 3, where the relative differences between calculated and crystallographic hydrogen bond distances are presented for hydrogen bond interactions a and d.

When comparing the results of all periodic calculations, the BP86/PW/4 and BP86/PW/16ab geometries fail in accuracy. In both structures, the N_3-H_6 bond length is overestimated by 0.06 Å and the dihedral angles show considerable discrepancies with the crystal structure. The former approach results in an overall rotation of $-9°$ for the amino group and the CO_2 group in the latter approach is 20° away from its original orientation in the crystal (see Table 1). These rotations reflect the incorrect prediction of hydrogen bond lengths in both methods. As is apparent from Figure 3, serious inaccuracies are obtained with respect to hydrogen bond interaction a: the O_4-H^a and H_6-O^a distances are seriously underestimated by at least 0.20 Å in BP86/PW/16ab and even 0.25 Å in BP86/PW/4. Due to the occurrence of such large errors, it must be concluded that the BP86/PW/4 and BP86/PW/16ab periodic approximations offer an inadequate reproduction of the glycine crystal structure. The origin of these effects must be traced back to the dimensions of the periodic supercell that are in both cases too small to prevent undesirable interactions between optimized molecules of neighboring cells. The BP86/PW/16bc approach gives a fairly good description of hydrogen bond interaction a. With a maximum deviation of 0.08 Å for H_6-O^a, this method is even quite comparable with the BP86/PW/16ac and BP86/PW/32 models. However, for the elongated O_5-H^d hydrogen bond length, the comparison no longer applies and the BP86/PW/16bc method must also be rejected.

Among all periodic models, it turns out that the BP86/PW/16ac and BP86/PW/32 approaches give the best description of all hydrogen bond interactions in the glycine crystal. Furthermore, in view of the large similarities between the latter two geometries, it can be safely assumed that the geometry of the optimized glycine molecule is already converged for the BP86/PW/16ac supercell approximation. In other words, the latter correspondence demonstrates that it is not necessary to enlarge the unit cell along its longest cell dimension (the b direction). This presents a confirmation for the periodic approach that was followed in an earlier study on L-α-alanine.[26]

From this initial model assessment it is clear that among the cluster methods a full ab initio (B3LYP/7) model emerges as the best to describe the intermolecular forces within the glycine solid state; the BP86/PW/16ac and BP86/PW/32 periodic approaches offer comparable accuracy. Hybrid cluster calculations (B3LYP/PM3/7) and periodic methods in which the periodic supercell is not adequately chosen (BP86/PW/4, BP86/PW/16ab-bc) present an incomplete and inadequate reproduction of the glycine crystal structure.

4. Impact of Model Space Approach on Radical Geometry

Because the $^+NH_3-{}^\bullet CH-CO_2^-$ radical is a fairly simple hydrogen abstraction product of glycine, it most likely will still bear some resemblance to the undamaged crystal structure. The major alteration is expected for the planarity of the C_2 carbon radical center, expressed by the $C_1-N_3-H_9-C_2$ improper

TABLE 2: Overview of Selected Geometrical Features for Optimized Radical Geometries[a]

		Optimized radical geometry									
		Single molecule		Cluster approach			Periodic approach				
	exptl	B3LYP/1	B3LYP/ Onsager/1	B3LYP/ PM3/7	B3LYP/ PM3/10	B3LYP/7	BP86/ PW/4	BP86/PW/ 16ab	BP86/PW/ 16ac	BP86/PW/ 16bc	BP86/PW/32
Bond Lengths											
C1−C2	1.527	1.468	1.501	1.448	1.440	1.469	1.459	1.458	1.450	1.448	1.450
C1−O4	1.257	1.257	1.266	1.267	1.264	1.268	1.278	1.283	1.290	1.288	1.290
C1−O5	1.259	1.259	1.270	1.280	1.276	1.265	1.297	1.292	1.291	1.298	1.292
C2−N3	1.482	1.505	1.471	1.490	1.484	1.438	1.416	1.415	1.437	1.434	1.437
C2−H9	1.080/1.090	1.078	1.083	1.081	1.101	1.080	1.084	1.085	1.083	1.082	1.084
N3−H6	1.036	1.036	1.034	1.047	1.044	1.049	1.109	1.113	1.076	1.082	1.076
N3−H7	1.024	1.024	1.036	1.061	1.065	1.055	1.078	1.073	1.078	1.095	1.077
N3−H8	1.024	1.024	1.034	1.064	1.059	1.044	1.049	1.051	1.051	1.045	1.051
Dihedral Angles											
O4−C1−C2−N3	19.5	19.0	0.0	29.7	24.8	15.2	13.2	20.8	15.2	14.6	14.4
O5−C1−C2−N3	−161.3	−161.6	−180.0	−145.0	−150.9	−161.6	−166.0	−158.5	−163.6	−166.4	−164.2
H6−N3−C2−C1	177.3	177.6	183.7	173.7	171.0	179.2	174.0	−175.7	178.0	170.9	178.5
H7−N3−C2−C1	−60.6	−59.5	−54.8	−63.0	−63.6	−56.6	−64.3	−53.7	−57.1	−68.6	−56.5
H8−N3−C2−C1	57.9	57.8	64.8	51.6	49.8	62.3	54.5	64.9	59.3	50.3	59.9
Improper Torsion Angles											
C2−O4−O5−C1	0.6	0.4	0.0	−3.0	−2.8	−2.2	−0.5	−0.5	−0.8	0.7	−0.9
C1−N3−H9−C2	−37.5/36.0	2.7	0.0	11.3	−7.7	7.0	2.3	4.6	1.5	−2.7	2.3
Hydrogen Bonding Distances											
O4−Ha	1.748			1.713	1.758	1.728	1.457	1.470	1.707	1.708	1.709
O4−Hb	2.387			2.320	2.253	2.364	2.520	2.591	2.417	2.438	2.412
O5−Hc	1.821			1.759	1.748	1.727	1.662	1.747	1.739	1.592	1.740
O5−Hd	2.040			1.834	1.763	1.969	2.222	2.010	2.088	2.315	2.082
H6−Oa	1.748			1.741	1.738	1.699	1.457	1.470	1.686	1.605	1.684
H7−Oc	1.821			1.812	1.748	1.764	1.662	1.697	1.685	1.592	1.686
H8−Od	2.040			1.819	1.858	1.994	2.068	2.006	2.091	2.155	2.095
H8−Ob	2.387			2.402	2.297	2.177	2.222	2.277	2.226	2.169	2.214

[a] The B3LYP/Onsager/1 geometry is taken from Ban et al. in ref 19.

torsional angle, due to the hydrogen loss. As a result of this perturbation, the CO_2 and NH_3 groups will be subject to minor adjustments.

4.1. Radical Geometry in Single-Molecule Approach. In Table 2, the main features of the optimized geometries have been characterized for all outlined methodologies. For completeness, we have also included information on the conformation proposed by Ban et al.,[19] labeled B3LYP/Onsager/1. This structure was also obtained at the DFT level of theory, using a B3LYP functional and a double-ζ 6-31+G** basis, within the Onsager solvent simulation approach.[23] The structure is quite similar to our single-molecule geometry, although a substantial deviation from the crystal structure is noticed for the CO_2 group. Both the $O_4-C_1-C_2-N_3$ and $O_5-C_1-C_2-N_3$ torsional angles give indication of an additional rotation of the CO_2 group of about 20°. In addition, a slight rotation of some 5° for the NH_3 group was suggested in order to get the closest fit between calculated and experimental EPR parameters. These geometrical features cannot be reproduced in our crude single-molecule approach because only C_2 and H_9 were allowed to relax.

4.2. Radical Geometry in Cluster Approach. Nearly identical bond lengths and dihedral angles can be observed for both ONIOM optimized structures. The hydrogen bond lengths in both the B3LYP/PM3/7 and B3LYP/PM3/10 geometries are also comparable to those of the crystal, the O_5-H^d and H_8-O^d distances notwithstanding. Apparently, the effects observed in the initial assessment on the optimized crystal geometry also apply here.

Only one feature is clearly differing in both ONIOM approaches: the $C_1-N_3-H_9-C_2$ dihedral angle, describing the planarity of the radical backbone, switches from +11.3° in the B3LYP/PM3/7 structure to −7.7° for B3LYP/PM3/10. This apparent incoherency as a result of cluster size expansion prompted us to investigate the effect of the radical planarity on the total cluster energy. In Figure 4 the total ONIOM extrapolated energies of both small (×) and large (◆) clusters are plotted as a function of the $C_1-N_3-H_9-C_2$ dihedral (relative to a base level of −284.83 au). In the upper and lower parts of the graph, distinct energetic minima are visible, roughly corresponding to the representative planarity values for the optimized B3LYP/PM3/7 and B3LYP/PM3/10 geometries, respectively. However, for the latter cluster, inconsistent energies are obtained for some specific $C_1-N_3-H_9-C_2$ values. This discontinuity in the ground-state energy behavior is obviously unphysical and needs special attention. We observe that in these specific unphysical cases, something wrong happens with the electronic PM3 wave function. An investigation of the spin density shows that a redistribution of the spin has taken place over different molecules in the cluster. Summing up all atomic spin densities per molecule, two molecules contribute to the total unpaired spin density ($\rho_\alpha - \rho_\beta$) with about +1/2 and −1/2, respectively, in addition to the +1/2 of the central radical. Although the net unpaired spin density of the complete cluster (1/2 in total) is still maintained in this scheme, a completely unphysical electronic configuration is thus obtained. Similar unphysical solutions with the PM3 method, in addition to convergence difficulties, were encountered in a preliminary study (taken up in ref 27) on even larger glycine clusters (including up to 18 molecules) and have also been recognized in a study of the cationic radicals in L-α-alanine.[45] Based on these indications of numerical instability with increasing cluster size and of the geometrical discrepancies with the B3LYP/PM3/7 structure, we decided to reject the B3LYP/PM3/10 optimized geometry altogether.

Comparing the full-B3LYP optimized geometry B3LYP/7 with the B3LYP/PM3/7 structure, several subtle, but striking differences can be noticed. Apart from an enhanced radical planarity (7.0° instead of 11.3° for $C_1-N_3-H_9-C_2$), the overall

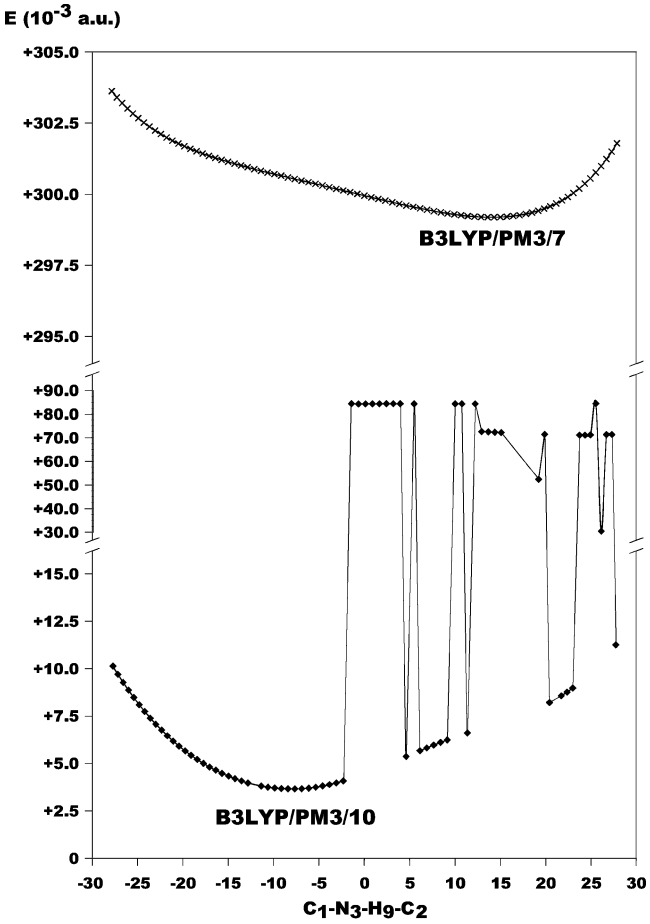

Figure 4. ONIOM extrapolated energies (in 10^{-3} au) of B3LYP/PM3/7 (×) and B3LYP/PM3/10 (◆) clusters, as a function of the $C_1-N_3-H_9-C_2$ dihedral angle. Energies are reported relative to a base level of −284.83 au.

rotation of the amino group is altered as well. Whereas in the B3LYP/PM3/7 structure, this group is rotated 4° about the N_3-C_2 bond in a clockwise direction with respect to the original crystal structure, in the B3LYP/7 structure it is rotated 4° in a counterclockwise direction, now in close agreement with the B3LYP/Onsager/1 geometry. A similar observation can be made for the CO_2 group rotation, which is now virtually parallel with its original orientation in the crystal for B3LYP/7. These effects are most likely correlated with a more correct description within DFT of the O_5-H^d and H_8-O^d weak hydrogen bonds between radical and lattice, as observed earlier in section 3. In fact, all geometrical features of the glycine radical and the optimized crystal are comparable, apart from the C_2-H_9 distance and the $C_1-N_3-H_9-C_2$ improper torsion angle, evidently.

4.3. Radical Geometry in Periodic Approach. The initial objective of performing the periodic calculations with different supercell sizes was to evaluate at what size radicals in adjacent cells are sufficiently separated. From this viewpoint, the BP86/PW/4, BP86/PW/16ab, and BP86/PW/16bc methods were a priori considered deficient, since these models contain one or more direct intermolecular contacts between radicals in adjacent cells: the hydrogen bonds of interaction a in BP86/PW/16ab, interaction c in BP86/PW/16bc, and both interactions in BP86/PW/4. The effect of these direct contacts is apparent in Table 2, where large differences with the original crystal structure are noticeable for the involved hydrogen bond lengths. These errors were already present in the optimized crystal geometries (Table 1) but are further enhanced in the radical geometries. The O_4-H^a and H_6-O^a distances in BP86/PW/4 and BP86/PW/16ab are now underestimated by some 0.28 Å while the O_5-H^c and H_7-O^c distances are shortened with 0.16 Å in BP86/PW/4 and 0.23 Å in BP86/PW/16bc. This seems to corroborate the shortcomings of these models as already concluded in section 3.

In view of the striking similarity between the remaining BP86/PW/16ac and BP86/PW/32 optimized radical geometries (Table 2), it can be concluded that a treatment using the former, smaller supercell size is already sufficient. This implies that radical defects are adequately separated when doubling the unit cell in the a and c directions, entirely validating the procedure adopted in an earlier study on L-α-alanine.[26] A closer inspection of the optimized radical geometry of either approach reveals that the structure is essentially planar (about 2° for the $C_1-N_3-H_9-C_2$ dihedral) and that the orientation of the CO_2 group is close to its original direction in the crystal. In the amino group, the $H_6-N_3-C_2-C_1$ and $H_8-N_3-C_2-C_1$ torsion angles display only minor changes. On the other hand, a small but noticeable deviation (4°) is visible for the $H_7-N_3-C_2-C_1$ dihedral, which is probably linked to the larger H_7-O^c hydrogen bond distance. Apart from this latter torsional angle and the radical planarity, the BP86/PW/16ac and BP86/PW/32 structures closely resemble the B3LYP/7 optimized radical geometry.

Taking into account the inadequacy of the BP86/PW/4 and BP86/PW/16ab-bc models and the virtual equivalence of the BP86/PW/16ac and BP86/PW/32 structures, in the next section only the calculated EPR parameters have been reported for the model involving the most extended model space, i.e., BP86/PW/32. For reference, the calculated resonance parameters for the other models are taken up as Supporting Information [S1].

5. EPR Parameters

In this section, we will compare the different experimental EPR results with calculated EPR parameters for all optimized geometries, as summarized in Table 3. Here, all hyperfine couplings are presented in MHz and the principal axes of the tensors are always given by means of direction cosines with respect to the orthogonal reference frame ⟨oa*bc⟩ of the crystal. For reference, we have also summarized the calculated EPR parameters, obtained in earlier theoretical (single molecule) studies. The UQCISD/1, B3LYP/CPCM/1, and B3LYP/Onsager/1 labels thus refer to the results of Barone et al.,[18] Rega et al.[20] and Ban et al.,[19] respectively.

The collected experimental data identify six hyperfine coupling tensors for the $^+NH_3-{}^\bullet CH-CO_2^-$ glycine radical: one carbon tensor, one nitrogen tensor and four proton tensors. To facilitate a further analysis, specific experimental results were selected from the vast amount of data, to which theoretical results were compared. Preference was given to the results of more recent studies, and also some experimental errors, identified in several publications, were taken under consideration. In the Supporting Information [S2], we supply a detailed account of these issues. In what follows, all calculated EPR results for C_2, N_3, H_6, and H_9 in the model radical will be compared with the C_{exp} tensor of Morton,[6] N_{exp} of Hedberg and Ehrenberg,[15] the $H_{exp}(\beta 1)$ signal of Collins and Whiffen,[7] and the $H_{exp}(\alpha)$ tensor measured by Sanderud and Sagstuen,[16] respectively.

Two studies report on the $\beta 2$- and $\beta 3$- coupling protons in the glycine radical species. An initial discrepancy for the $H_{exp}(\beta 2)$ and $H_{exp}(\beta 3)$ principal axes between the Collins and Whiffen paper[7] and that of Sanderud and Sagstuen[16] was in part resolved by correcting for a typographical error in the latter study.[46] However, in view of the residual difference between these tensors in both articles and in order to present the analysis of the theoretical EPR parameters without any bias, we have

TABLE 3: Calculated EPR Parameters for All Optimized Radical Geometries[a]

	Experimental data																						Earlier theoretical studies			
	Ghosh & Whiffen (1959)					Morton (1964)					Collins & Whiffen (1966)					Hedberg & Ehrenberg (1968)					Sanderud & Sagstuen (1998)					UQCISD/1	B3LYP/CPCM/1	B3LYP/Onsager/1	
	Aiso	Taniso	Principal axes			Aiso	Taniso	Principal axes			Aiso	Taniso	Principal axes			Aiso	Taniso	Principal axes			Aiso	Taniso	Principal axes			Aiso	Aiso	Aiso	Taniso
C_{exp}							-90.0	0.902	-0.080	-0.424																			
						126.7	-36.7	0.360	-0.404	0.841																127.8	120.5	98.7	-74.6
							126.8	0.239	0.911	0.335																			150.9
N_{exp}	-8.6	3.4	-0.650	0.760	0.000							1.9	-0.394	0.916	-0.076		1.7	-0.217	0.951	0.219									-0.4
		-1.5	0.000	0.000	1.000						-9.0	-0.9				-8.7	-0.8	0.885	0.097	0.456						-12.3	-9.0	-7.0	0.2
		-2.0	-0.760	-0.650	0.000							-1.1					-1.0	-0.412	-0.293	0.863									0.2
$H_{exp}(\beta 1)$												-7.3	0.620	-0.680	0.391														-5.4
											3.3	-1.8	0.614	0.731	0.296											-	-	2.3	-4.7
												9.2	-0.488	0.057	0.871														10.1
$H_{exp}(\beta 2)$												-6.0	0.005	-0.810	0.587							-6.4	-0.077	-0.976	0.206				-5.5
											62.0	-3.2	0.146	0.581	0.801						62.0	-3.8	0.031	0.204	0.978	-	-	77.1	-4.5
												9.3	0.989	-0.082	-0.121							10.2	0.997	-0.081	-0.015				10.0
$H_{exp}(\beta 3)$												-6.1	0.751	0.361	0.551							-7.1	0.725	0.387	0.570				-5.5
											82.0	-4.0	-0.371	-0.460	0.807						83.1	-3.5	-0.386	-0.457	0.801	-	-	77.1	-4.5
												10.1	0.545	-0.811	-0.212							10.6	0.570	-0.801	-0.182				10.0
$H_{exp}(\alpha)$	-66.0	34.3	0.680	-0.630	0.370							27.3	0.789	-0.316	0.527		30.4	0.778	-0.378	0.502		31.9	0.797	-0.301	0.524				-36.1
		-4.4	0.430	0.750	0.500						-66.3	4.9	0.358	0.933	0.023	-63.5	2.2	0.412	0.910	0.047	-63.7	1.9	0.330	0.943	0.040	-72.3	-62.2	-59.0	-1.5
		-29.9	-0.600	0.180	0.780							-32.3	-0.499	0.171	0.850		-32.6	-0.475	0.170	0.864		-33.8	-0.507	0.141	0.851				37.5

	Calculated data																											
	B3LYP/1					B3LYP/PM3/7					B3LYP/PM3/7 (full)					B3LYP/7					B3LYP/7 (full)					BP86/PW/32				
	Aiso	Taniso	Principal axes			Aiso	Taniso	Principal axes			Aiso	Taniso	Principal axes			Aiso	Taniso	Principal axes			Aiso	Taniso	Principal axes			Aiso	Taniso	Principal axes		
C_2		-70.9	0.868	-0.368	-0.335		-63.5	0.677	-0.490	-0.549		-74.2	0.592	-0.392	-0.705		-70.3	0.713	-0.357	-0.603		-74.8	0.737	-0.352	-0.577		-67.6	0.719	-0.341	-0.606
	77.3	-69.9	0.191	-0.376	0.907	64.6	-62.7	0.434	-0.336	0.836	89.7	-73.7	0.539	-0.457	0.707	72.4	-68.8	0.551	-0.246	0.797	77.8	-73.4	0.512	-0.266	0.817	68.7	-66.2	0.520	-0.314	0.794
		140.8	0.459	0.851	0.256		126.2	0.594	0.804	0.015		147.9	0.599	0.798	0.059		139.1	0.433	0.901	-0.022		148.2	0.441	0.897	0.015		133.9	0.461	0.886	0.049
N_3		-0.5	0.266	-0.276	0.924		-0.4	0.657	-0.366	0.659		-1.6	-0.767	0.637	0.076		-0.6	0.599	-0.154	0.786		-1.4	0.592	-0.322	0.739		-0.6	0.724	0.115	0.680
	-7.1	0.1	0.580	-0.719	-0.382	-8.3	0.1	0.535	0.843	-0.065	-6.2	-1.2	0.059	-0.048	0.997	-10.2	-0.1	0.386	0.915	-0.115	-7.4	-1.0	0.640	-0.370	-0.673	-8.9	-0.1	0.190	0.915	-0.356
		0.4	0.770	0.638	-0.031		0.3	-0.532	0.395	0.749		2.9	0.639	0.769	-0.001		0.6	-0.701	0.372	0.608		2.4	0.490	0.872	-0.013		0.7	-0.664	0.387	0.640
H_6		-5.3	0.370	-0.540	0.756		-4.7	0.583	-0.588	0.561		-5.1	0.532	-0.710	0.462		-5.2	0.691	-0.440	0.574		-5.1	0.615	-0.639	0.462		-4.8	0.662	-0.496	0.562
	2.2	-3.8	0.489	0.805	0.336	3.5	-3.4	0.674	0.735	0.071	0.9	-4.1	0.766	0.636	0.096	6.6	-3.8	0.499	0.864	0.062	2.4	-4.3	0.667	0.734	0.128	3.4	-3.6	0.520	0.844	0.132
		9.0	-0.790	0.245	0.562		8.1	-0.454	0.337	0.825		9.2	-0.362	0.303	0.881		9.0	-0.523	0.244	0.817		9.4	-0.421	0.229	0.878		8.4	-0.540	0.205	0.816
H_7		-4.9	-0.274	-0.936	0.223		-4.7	-0.462	-0.764	-0.452		-7.2	-0.234	-0.858	0.457		-4.8	-0.138	-0.936	0.323		-7.1	-0.092	-0.901	0.423		-4.4	-0.247	-0.945	-0.215
	57.3	-4.4	-0.057	0.247	0.967	53.1	-4.2	0.026	-0.520	0.854	54.3	-3.6	0.216	0.413	0.885	65.0	-4.5	0.269	0.278	0.922	56.7	-3.8	0.097	0.415	0.905	80.6	-4.0	0.188	-0.265	0.946
		9.3	0.960	-0.252	0.121		8.9	0.887	-0.382	-0.260		10.8	0.948	-0.306	-0.088		9.3	0.953	-0.214	-0.213		10.8	0.991	-0.124	-0.049		8.4	0.951	-0.193	-0.243
H_8		-6.1	0.218	0.159	0.963		-5.0	0.667	0.119	0.735		-7.0	0.772	0.194	0.605		-5.9	0.539	0.105	0.835		-7.3	0.678	0.237	0.696		-5.8	0.522	0.147	0.840
	59.6	-4.2	-0.729	-0.630	0.269	66.3	-3.7	-0.573	-0.549	0.609	70.7	-3.7	-0.528	-0.333	0.781	92.7	-3.9	-0.580	-0.673	0.459	93.6	-4.0	-0.545	-0.473	0.692	81.7	-3.8	-0.567	-0.676	0.471
		10.3	0.649	-0.760	-0.021		8.7	0.476	-0.827	-0.299		10.7	0.353	-0.923	-0.154		9.8	0.610	-0.732	-0.302		11.3	0.493	-0.848	-0.191		9.6	0.637	-0.723	-0.270
H_9		-33.9	-0.777	0.217	0.592		-29.7	-0.456	0.290	0.842		-35.8	-0.481	0.287	0.828		-33.1	-0.492	0.226	0.841		-36.0	-0.517	0.232	0.824		-31.4	-0.505	0.189	0.842
	-56.4	-2.2	0.471	0.824	0.316	-42.0	-2.9	0.603	0.796	0.053	-50.2	-3.4	0.568	0.822	0.045	-53.7	-2.5	0.442	0.897	0.017	-57.2	-3.0	0.426	0.905	0.013	-54.0	-2.6	0.496	0.862	0.104
		36.1	0.419	-0.524	0.742		32.6	0.655	-0.532	0.537		39.2	0.668	-0.493	0.558		35.6	0.750	-0.380	0.541		39.1	0.743	-0.358	0.566		34.0	0.706	-0.470	0.530

[a] A summary is also presented of relevant EPR parameters reported in earlier experimental (refs 5, 6, 7, 14, and 15) and theoretical studies (refs 17, 19, and 18).

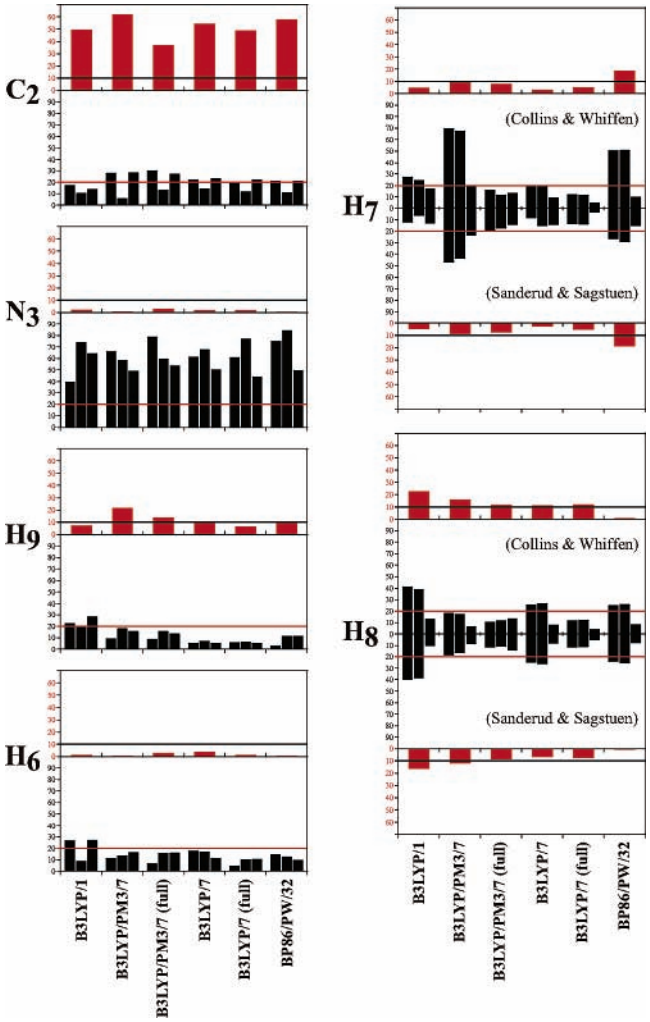

Figure 5. Experimental versus calculated hyperfine tensors for the geometries obtained at various levels of theory. Absolute differences (in MHz) between calculated and experimental isotropic hyperfine couplings are represented as red bars at the top of each graph. The deviations of the measured and predicted hyperfine tensor principal directions (in degrees) are given as black bars, with (from left to right) minor, intermediate and major anisotropic eigenvalues.

preferred to compare the theoretical EPR parameters of H_7 and H_8 with the results of both experimental studies.

All relevant calculated EPR data are also displayed in Figure 5. The red bars at the top of each plot represent the absolute difference (in MHz) between the experimental hyperfine coupling constants and the calculated values for the optimized geometries, obtained at various levels of theory. The deviation (in degrees) of the three calculated hyperfine principal directions with the three corresponding experimental directions is schematically presented as black bars at the bottom of each plot. Although several studies[47] have focused on the correct reproduction of the hyperfine coupling constants, we also emphasize the importance of reproducing the hyperfine tensor principal axes. The presence of a Fermi contact term in the expression of the hfcc[22] makes this parameter very sensitive to the level of theory. The principal axes on the other hand do not depend on this term, and the requirement of complicated, high-level calculations with extended basis sets (e.g., EPR−III[21]) may be less important. As will become apparent, however, the accuracy of the axes depends largely on the completeness of the model space.

To systematically retain or reject a theoretical procedure for the reproduction of EPR data, that is, both hyperfine couplings and tensor axes, we introduced two criteria that accepted methods must fulfill. For the isotropic couplings, a maximum deviation of 10 MHz is accepted (criterion I), to account for the only limited basis set used in the EPR calculation. In a previous study on fructose,[44] an improvement of 10 MHz was observed when switching from 6−311G** to a more extended basis set (EPR-III) on the same carbohydrate geometry. Similar corrections are also found in other studies.[48] A deviation of 20° at most is assumed to be acceptable for the tensor axes (criterion II). This limit is based on the maximum deviation between the Sanderud−Sagstuen and Collins−Whiffen experiments for the $H_{exp}(\beta 2)$ tensor axes corresponding to the minor and intermediate anisotropic coupling. The thresholds of both criteria are indicated in Figure 5 by horizontal lines. A model approach that violates either of these criteria must be considered as unable to reproduce the experimental data in a satisfactory way. As a result, they have been assessed in function of criteria I and II.

5.1. Single-Molecule Calculations. Based solely on isotropic hyperfine coupling constants, the B3LYP/1 conformer offers a moderate agreement with experimental data. For the C_2 and H_8 couplings, substantial deviations (about 50 and 20 MHz, respectively) are observed, violating criterion I. The calculated couplings are furthermore quite similar to those predicted in earlier single-molecule calculations (see Table 3), apart from the C_2 carbon coupling which is seriously underestimated in our B3LYP/1 calculation but nicely reproduced by the UQCISD/1 and B3LYP/CPCM/1. This disagreement looks somewhat surprising but is due to vibrational averaging effects, which are taken into account in the latter two studies. The B3LYP/Onsager/1 model of Ban et al.[19] and our B3LYP/1 approach both predict almost identical couplings. The reproduction of the hfccs for the H_7 and H_8 amino protons (77 versus 60 MHz) sounds a little bit better in the B3LYP/Onsager/1 model, which can be traced back to the additional rotation of the amino group about the C_2-N_3 bond. This internal rotation was not the direct result of a geometry optimization but rather was artificially imposed to give an indication of how the rotation of the amino group may improve the agreement with experiment.

Moreover, the B3LYP/1 geometry does not succeed in predicting overall satisfactory principal hyperfine directions. Large discrepancies are noticeable and criterion II is violated in all but two cases. A quite good agreement is found with the C_{exp} directions and for H_7. The calculated principal axes differ only 10° from those of the $H_{exp}(\beta 2)$ tensor measured by Sanderud and Sagstuen.[16] The largest deviations from experiment, on the other hand, are obtained for the N_3 and H_8 principal axes. They can rise up to 70° and more.

If we consider the proton EPR parameters in particular as key probes for the accuracy of the proposed structure, a poor result is achieved since both criteria I and II are not met for the H_8 proton. Therefore, the B3LYP/1 geometry must be rejected as it does not yield a good prediction of the EPR data for the considered glycine radical.

5.2. Cluster Calculations − B3LYP/PM3/7 and B3LYP/7. In comparison with the very simplified single-molecule approach, an important improvement is obtained for the H_7 and H_8 isotropic hyperfine coupling constants in both the B3LYP/PM3/7 and B3LYP/7 cluster calculations. The latter geometry almost perfectly reproduces the experimentally observed difference in coupling constants (20 MHz). On the other hand, the B3LYP/PM3/7 geometry fails for the α-hydrogen (H_9) and the C_2 coupling. Apart from the particular C_2 hyperfine

interaction, B3LYP/7 is the only level of theory able to predict isotropic coupling values that meet criterion I.

A similar discussion can be held on the reproduction of the hyperfine principal directions. The deviations from experiment are given by the black bars in Figure 5. The cluster calculations are completely missing the hyperfine principal axes for the nitrogen atom N_3, but on the other hand nicely succeed in predicting the axes for the four hydrogen atoms. One large discrepancy attracts attention: the two axes belonging to the two minor anisotropic coupling components predicted for the H_7 proton in the B3LYP/PM3/7 approach. The orientations of these axes differ by more than 45° from experiment (either Collins and Whiffen[7] or Sanderud and Sagstuen[16]). However, we notice that the minor and intermediate anisotropic coupling eigenvalues are close to degeneracy (−4.2 versus −4.7 MHz). Eigenvectors of degenerate eigenvalues are not uniquely determined. Only the plane of the axes perpendicular to the principal axis corresponding to the major (nondegenerate) eigenvalue (+8.9 MHz) is completely defined, and this plane seems to be reproduced within the 20° threshold of criterion II.

This is a striking phenomenon, which also arises at other levels of theory: one component (corresponding to the largest T_{aniso}), which is in excellent agreement with experiment, and the two minor components exhibiting large, but equal discrepancies with experiment. In all these cases, the two minor T_{aniso} values are close to each other, generating large inaccuracies in the determination of the eigenvectors. A simple rotation of the last two principal axes about the former well determined axis would be sufficient to get an excellent reproduction of all hyperfine principal directions.

5.3. Cluster Calculations − B3LYP/PM3/7(full) and B3LYP/7(full). In an attempt to break this quasi-degeneracy, the size of the model space in the EPR calculation was increased. This is achieved by taking explicitly into account the nearest molecular environment of the radical for the evaluation of the EPR parameters. The results are labeled B3LYP/PM3/7(full) and B3LYP/7(full) and were obtained by performing additional EPR calculations on the entire B3LYP/PM3/7 and B3LYP/7 optimized cluster geometries (not just the radical). What could be expected indeed happens: the degeneracy of the two lowest eigenvalues of the T_{aniso} tensor is completely removed, and the agreement with experiment becomes excellent. This spectacular change is observed for H_7 in B3LYP/PM3/7(full), for H_8 in B3LYP/7(full), and to a lesser degree for H_6 in B3LYP/7(full). As is visible in Figure 5, criterion II is well met for these protons.

All discussed cluster approaches utterly fail to correctly predict the N_3 nitrogen hyperfine tensor principal directions. In addition, any sign of improvement is indiscernible when increasing the size of the model space in the EPR calculation (e.g., comparing the B3LYP/PM3/7 and B3LYP/7(full) results). This suggests either that DFT is inadequate to calculate nitrogen hyperfine tensor axes, or that an ambiguity persists in the description of the experimental tensor principal directions. Taking into account the satisfactory reproduction of the nitrogen hyperfine coupling constant using DFT methods on one hand and the contradictions between the different experimental studies concerning the nitrogen tensor axes on the other, we tend to assume the latter suggestion to be correct.

The enlargement of the model space has also a beneficial influence on the reproduction of the C_2 isotropic coupling constant: the value of 64.6 MHz is raised to 87.7 MHz in B3LYP/PM3/7(full). This isotropic carbon coupling is still too small however to achieve criterion I, but as similar low values are reported throughout all other calculations, this can be attributed to the only moderate basis size, as opposed to the more specialized basis sets (EPR-II) used in, for instance, the B3LYP/CPCM/1 approach.[20] Another contributing factor to the underestimation of this coupling is the absence of any temperature consideration in our model approaches. Since calculations are performed at 0 K in a vacuum, temperature effects, such as vibrational averaging motions treated in the B3LYP/CPCM/1 and UQCISD/1 models, are not taken into account. As reported in refs 18 and 27, these effects will also significantly improve the isotropic hyperfine coupling constants of C_2, as well as of H_9. All other reported couplings remain quite comparable. The best agreement for all protons is obtained within the B3LYP/7(full) cluster approach, which makes sense considering the superior size of the model space.

The improvement of the calculated hyperfine directions restricts to some extent the validity of the observation formulated in ref 20 that "the magnetic properties of a glycine radical in its zwitterionic form are scarcely affected by the crystalline environment". As corroborated by the differences between the B3LYP/7 and B3LYP/7(full) calculations, only the (proton) hyperfine couplings are largely unaffected by the presence of a crystal lattice, but this may not be extended to the hyperfine principal directions, where a more elaborate description of the surrounding may lift the possible degeneracy, leading to a more accurate determination of the axes.

5.4. Periodic Calculations. Criterion I is not fulfilled for the structure resulting from the BP86/PW/32 calculations. Apart from the difference with the C_{exp} coupling, common to all calculations, an error of up to 20 MHz also appears for the H_7 proton. This is most likely connected with the peculiar asymmetric modification of the amino group, as expressed by the $H_7-N_3-C_2-C_1$ dihedral angle (see section 4.3). The erroneously predicted H_7 hfcc also distorts the qualitative coupling scheme as the NH_3 group of the BP86/PW/32 glycine radical is now characterized by two large couplings of about 80 MHz in addition to one small coupling. Furthermore, the predicted hyperfine tensor principal directions for this amino proton also largely deviate from the experimental principal axes, although the deviation for the component corresponding to the largest T_{aniso} is well below 20°, thus meeting criterion II. Essentially, the deviations of the hyperfine tensor axes for the protons of the BP86/PW/32 structure are quite comparable with those of the B3LYP/7 calculation. The degeneracy of the two minor Taniso values reappears for H_8 and H_7, and the predicted direction cosines for H_9 and H_6 are in close agreement with experiment. At this point, we want to stress that the EPR parameters in the periodic approach are obtained by performing calculations on the single radical of which the geometry was obtained by the periodic calculations. Up to now, no program packages are available that allow the calculation of EPR data using the full model space, that is, using the wave functions that are expressed as an expansion in plane waves. Such calculations would likely cause an improvement, similar to the amelioration of the B3LYP/7 results in the B3LYP/7(full) calculation. Further model development is therefore needed for this type of plane wave calculations and is currently in progress in our research group.

Most notably, a comparison between the BP86/PW/32 and B3LYP/7 spectroscopic properties reveals that the EPR parameters for the α-proton H_9 in both approximations are in equally good correspondence with experiment. Therefore, it cannot be established from our theoretical calculations whether the radical backbone is actually planar (as indicated by the periodic

approach) or not (as suggested by the cluster calculation). This would be consistent with the suggestion in several single-molecule studies[18,20] that the H_9 proton is subject to thermal vibrations.

6. Conclusions

In this work, we have computed the geometries and EPR parameters of the $^{+}NH_3-{}^{\bullet}CH-CO_2^{-}$ radiation-induced radical of α-glycine in the solid state. Several model spaces were considered, including a single-molecule approach, cluster models, and periodic calculations, all based on density functional theory. The structural characteristics of the obtained geometries have been compared with the experimental values obtained from X-irradiated crystals of α-glycine at 23 K.

In an initial assessment of the efficiency for each approach, it was found that the level of theory has a most distinct effect on the description of hydrogen bonds interconnecting adjacent glycine molecules within the crystal. It was established that a full ab initio cluster model or periodic calculations with properly enlarged unit cells are the most favorable methods. In addition, it was found that care must be taken in the construction of the supercell in a periodic approach. Enlargement of the original crystal unit cell is essential but seems not to be required along the longest cell dimension (direction b).

Subsequently, these methods were applied to determine the optimal geometry of the glycine radical within the crystal. In this application, however, a correct description of hydrogen bond interactions appears essential to yield representative EPR parameters for the glycine amino protons, whose internal rotation with respect to the crystal is mainly determined by hydrogen bonding forces.

In an ensuing, comprehensive study of the EPR parameters, calculated on the optimized geometries, both the hyperfine coupling constants and the hyperfine tensor principal directions were cross-referenced with selected data, taken from a wealth of (albeit sometimes rather old) experimental studies on glycine. In general, the isotropic hyperfine couplings are not exactly reproduced, and in the BP86/PW/32 approach not even a qualitative agreement is acquired. Especially the calculated isotropic carbon couplings are only a fraction of the actual experimental value. According to the literature, these deviations must be attributed to other factors such as temperature effects or basis size effects. Since the trends observed for the calculated isotropic hyperfine constants could be transferred to the anisotropic couplings, they have consequently not been dealt with in detail.

In this paper, the relevance of a good reproduction of the hyperfine tensor principal axes has been stressed. It can be regarded as a sensitive probe for the accuracy of the proposed methodology to describe the glycine radical. Few levels of theory turn out to reproduce the experimental hyperfine principal directions in a satisfactory way. Only the B3LYP/7 and to some extent the BP86/PW/32 methods were able to achieve this goal. In the case of the former approach, this agreement was substantially further improved by also incorporating the explicit molecular environment of the complete cluster model in the EPR calculations. Predominantly in the case of a quasi-degeneracy of the two lowest eigenvalues of the anisotropic tensor for the β-protons, the enlargement of the model space removes the degeneracy and predicts the axes of the two nearly degenerate values within 10−15° from the experimental directions. For the periodic approach, so far no packages exist that allow similar periodic EPR calculations.

The best overall agreement between theory and experiment is observed for the B3LYP/7(full) calculations. The isotropic coupling constants are in fair accordance with experiment (except for the C_{exp} coupling) and the hyperfine tensor principal directions deviate not much from the experimental ones, in particular for the protons where the agreement is very good (always below 13° deviation) and also for C_2, where the agreement is moderate (never more than 22°). The N_{exp} principal axes are by far not reproduced by any of the proposed models. A possible explanation for this failure lies in the inconsistencies in the experimental data. Large discrepancies are noticed between the various experiments, which make the validity of the nitrogen tensor data questionable.

Acknowledgment. This work is supported by the Fund for Scientific Research − Flanders (FWO) and the Research Board of the Ghent University. The authors thank Audun Sanderud for providing a rectification of the glycine hyperfine tensor data, originally reported in ref 16.

Supporting Information Available: [S1]Overview of calculated EPR parameters for periodic models BP86/PW/4, BP86/PW/16ab, BP86/PW/16ac, and BP86/PW/16bc. [S2]Comments on selection between particular experimental results. [S3]-Optimized structures, obtained at all levels of theory, given in Cartesian coordinates. This material is available free of charge via the Internet at http://pubs.acs.org.

References and Notes

(1) As an example of a reference work, see: Box, H. C. *Radiation Effects: ESR and ENDOR Analysis*; Academic Press: New York, 1977.
(2) For an overview, see, e.g., Stubbe, J.; van der Donk, W. A. *Chem. Rev.* **1998**, *98*, 705.
(3) Gordy, W.; Ard, W. B.; Shields, H. *Natl. Acad. Sci. U.S.A.* **1955**, *41*, 983.
(4) Combrisson, J.; Uebersfeld, J. *Compt. Rend.* **1954**, *238*, 1397. Uebersfeld, J.; Erb, E. *Compt. Rend.* **1956**, *243*, 478.
(5) Ghosh, D. K.; Whiffen, D. H. *Mol. Phys.* **1959**, *2*, 285.
(6) Morton, J. R. *J. Am. Chem. Soc.* **1964**, *86*, 2325.
(7) Collins, M. A.; Whiffen, D. H. *Mol. Phys.* **1966**, *10*, 317.
(8) Symons, M. C. R. *J. Chem. Soc.* **1959**, 277.
(9) Box, H. C.; Freund, H. G.; Budzinski, E. E. *J. Am. Chem. Soc.* **1966**, *88*, 658. Teslenko, V. V.; Gromovoi, Y. S.; Krivenko, V. G. *Mol. Phys.* **1975**, *30*, 425.
(10) Deigen, M. F.; Krivenko, V. G.; Pulatova, M. K.; Ruban, M. A.; Teslenko, V. V.; Kayushin, L. P. *Biofizika* **1973**, *18*, 235. Iwasaki, M.; Muto, H. *J. Chem. Phys.* **1974**, *61*, 5315. Nunome, K.; Muto, H.; Toriyama, K.; Iwasaki, M. *J. Chem. Phys.* **1976**, *65*, 3805. Muto, H.; Iwasaki, M.; Takahashi, Y. *J. Chem. Phys.* **1977**, *66*, 1943. Smith, C. J.; Poole, C. P.; Farach, H. A. *J. Chem. Phys.* **1981**, *74*, 993. Syutkin, V. M.; Tolkatchev, V. A. *Chem. Phys. Lett.* **1985**, *122*, 201. Chis, V.; Brustolon, M.; Morari, C.; Cozar, O.; David, L. *J. Mol. Struct.* **1999**, *483*, 283.
(11) Brustolon, M.; Chis, V.; Maniero, A. L.; Brunel, L.-C. *J. Phys. Chem. A* **1997**, *101*, 4887.
(12) Neta, P.; Fessenden, R. W. *J. Phys. Chem.* **1971**, *75*, 738.
(13) Turecek, F.; Carpenter, F. H. *J. Chem. Soc., Perkins Trans. 2* **1999**, *11*, 2315. Turecek, F.; Carpenter, F. H.; Polce, M. J.; Wesdemiotis, C. *J. Am. Chem. Soc.* **1999**, *121*, 7955.
(14) Sagstuen, E.; Sanderud, A.; Hole, E. O. *Radiat. Res.* **2004**, *162*, 112.
(15) Hedberg, A.; Ehrenberg, A. *J. Chem. Phys.* **1968**, *48*, 4822.
(16) Sanderud, A.; Sagstuen, E. *J. Phys. Chem. B* **1998**, *102*, 9353.
(17) Ding, Y.; Krogh−Jespersen, K. *Chem. Phys. Lett.* **1992**, *199*, 261.
(18) Barone, V.; Adamo, C.; Grand, A.; Subra, R. *Chem. Phys. Lett.* **1995**, *242*, 351.
(19) Ban, F.; Gauld, J. W.; Boyd, R. J. *J. Phys. Chem. A* **2000**, *104*, 5080.
(20) Rega, N.; Cossi, M.; Barone, V. *J. Am. Chem. Soc.* **1998**, *120*, 5723.
(21) Barone, V. In *Recent Advances in Density Functional Methods, Part I*; Chong, D. P., Ed.; World Scientific: Singapore, 1995; Chapter 8.
(22) Malkin, V. G.; Malkina, O. L.; Eriksson, L. A.; Salahub, D. R. In *Modern Density Functional Theory: A Tool for Chemistry*; Pulitzer, P.; Seminario, J. M., Eds.; Elsevier: Amsterdam, 1995; Chapter 9.
(23) Onsager, L. *J. Am. Chem. Soc.* **1936**, *58*, 1486. Wong, M. W.; Frisch, M. J.; Wiberg, K. B. *J. Am. Chem. Soc.* **1991**, *113*, 4776. Wong, M. W.; Wiberg, K. B.; Frisch, M. J. *J. Chem. Phys.* **1991**, *95*, 8991. Wong,

M. W.; Wiberg, K. B.; Frisch, M. J. *J. Am. Chem. Soc.* **1992**, *114*, 523. Wong, M. W.; Wiberg, K. B.; Frisch, M. J. *J. Am. Chem. Soc.* **1992**, *114*, 1645.

(24) Pauwels, E.; Van Speybroeck, V.; Vanhaelewyn, G.; Callens, F.; Waroquier, M. *Int. J. Quantum Chem.* **2004**, *99*, 102.

(25) Saebo, S.; Klewe, B.; Samdal, S. *Chem. Phys. Lett.* **1983**, *97*, 499.

(26) Pauwels, E.; Van Speybroeck, V.; Lahorte, P.; Waroquier, M. *J. Phys. Chem. A* **2001**, *105*, 8794.

(27) Van Speybroeck, V.; Pauwels, E.; Stevens, F.; Callens, F.; Waroquier, M. *Int. J. Quantum Chem.*, accepted for publication.

(28) Car, P.; Parrinello, M. *Phys. Rev. Lett.* **1985**, *55*, 2471.

(29) Improta, R.; Barone, V. *Chem. Rev.* **2004**, *104*, 1231.

(30) Destro, R.; Roversi, P.; Barzaghi, M.; Marsh, R. E. *J. Phys. Chem. A* **2000**, *104*, 1047.

(31) Gaussian 03, Revision B.03, Frisch, M. J.; Trucks, G. W.; Schlegel, H. B.; Scuseria, G. E.; Robb, M. A.; Cheeseman, J. R.; Montgomery, J. A., Jr., Vreven, T.; Kudin, K. N.; Burant, J. C.; Millam, J. M.; Iyengar, S. S.; Tomasi, J.; Barone, V.; Mennucci, B.; Cossi, M.; Scalmani, G.; Rega, N.; Petersson, G. A.; Nakatsuji, H.; Hada, M.; Ehara, M.; Toyota, K.; Fukuda, R.; Hasegawa, J.; Ishida, M.; Nakajima, T.; Honda, Y.; Kitao, O.; Nakai, H.; Klene, M.; Li, X.; Knox, J. E.; Hratchian, H. P.; Cross, J. B.; Adamo, C.; Jaramillo, J.; Gomperts, R.; Stratmann, R. E.; Yazyev, O.; Austin, A. J.; Cammi, R.; Pomelli, C.; Ochterski, J. W.; Ayala, P. Y.; Morokuma, K.; Voth, G. A.; Salvador, P.; Dannenberg, J. J.; Zakrzewski, V. G.; Dapprich, S.; Daniels, A. D.; Strain, M. C.; Farkas, O.; Malick, D. K.; Rabuck, A. D.; Raghavachari, K.; Foresman, J. B.; Ortiz, J. V.; Cui, Q.; Baboul, A. G.; Clifford, S.; Cioslowski, J.; Stefanov, B. B.; Liu, G.; Liashenko, A.; Piskorz, P.; Komaromi, I.; Martin, R. L.; Fox, D. J.; Keith, T.; Al-Laham, M. A.; Peng, C. Y.; Nanayakkara, A.; Challacombe, M.; Gill, P. M. W.; Johnson, B.; Chen, W.; Wong, M. W.; Gonzalez, C.; Pople, J. A. Gaussian, Inc.: Pittsburgh, PA, 2003.

(32) For an example of a reference work, see: Parr, R. G.; Yang, W. *Density-Functional Theory of Atoms and Molecules*; Oxford University Press: New York, 1989.

(33) Becke, A. D. *J. Chem. Phys.* **1996**, *104*, 1040.

(34) Pauwels, E.; Van Speybroeck, V.; Waroquier, M. *Int. J. Quantum Chem.* **2003**, *91*, 511.

(35) Wong, M. W.; Radom, L. *J. Phys. Chem. A* **1998**, *102*, 2237. Parker, C. L.; Cooksy, A. L. *J. Phys. Chem. A* **1998**, *102*, 6186. Smith, D. M.; Nicolaides, A.; Golding, B. T.; Radom, L. *J. Am. Chem. Soc.* **1998**, *120*, 10223. Lynch, B. J.; Fast, P. L.; Harris, M.; Truhlar, D. G. *J. Phys. Chem. A* **2000**, *104*, 4811. Van Speybroeck, V.; Van Neck, D.; Waroquier, M.; Wauters, S.; Saeys, M.; Marin, G. B. *J. Phys. Chem. A* **2000**, *104*, 10939.

(36) Krishnan, R.; Binkley, J. S.; Seeger, R.; Pople, J. A. *J. Chem. Phys.* **1980**, 72, 650. McLean, A. D.; Chandler, G. S. *J. Chem. Phys.* **1980**, 72, 5639.

(37) Maseras, F.; Morokuma, K. *J. Comput. Chem.* **1995**, *16*, 1170. Svensson, M.; Humbel, S.; Froese, R. D. J.; Matsubara, T.; Sieber, S.; Morokuma, K. *J. Phys. Chem.* **1996**, *100*, 19357. Humbel, S.; Sieber, S.; Morokuma, K. *J. Chem. Phys.* **1996**, *105*, 1959. Matsubara, T.; Sieber, S.; Morokuma, K. *Int. J. Quantum Chem.* **1996**, *60*, 1101. Dapprich, S.; Komaromi, I.; Byun, K. S.; Morokuma, K.; Frisch, M. J. *J. Mol. Struct. (THEOCHEM)* **1999**, *462*, 1.

(38) Stewart, J. J. P. *J. Comput. Chem.* **1989**, *10*, 209. Stewart, J. J. P. *J. Comput. Chem.* **1989**, *10*, 221.

(39) Hutter, J.; Ballone, P.; Bernasconi, M.; Focher, P.; Fois, E.; Goedecker, S.; Parrinello, M.; Tuckermann, M. E., CPMD, version 3.7. Copyright IBM Corp. 1990−2003, Copyright MPI fuer Festkoerperforschung Stuttgart 1997−2001.

(40) Perdew, J. P. *Phys. Rev. B* **1986**, *33*, 8822. Becke, A. D. *J. Chem. Phys.* **1992**, *96*, 2155.

(41) Vanderbilt, D. *Phys. Rev. B* **1990**, *41*, 7892.

(42) Atherton, N. M. *Principles of Electron Spin Resonance*; Ellis Horwood, Prentice Hall: New York, 1993. Weil, J. A.; Bolton, J. R.; Wertz, J. E. *Electron Paramagnetic Resonance: Elementary Theory and Practical Applications*; Wiley-Interscience: New York, 1994.

(43) Kaupp, M.; Bühl, M.; Malkin, V. G. *Calculation of NMR and EPR Parameters − Theory and Applications*; Wiley-VCH: Weinheim, 2004.

(44) Pauwels, E.; Lahorte, P.; Vanhaelewyn, G.; Callens, F.; De Proft, F.; Geerlings, P.; Waroquier, M. *J. Phys. Chem. A* **2002**, *106*, 12340.

(45) Petrenko, T. L. *J. Phys. Chem. A* **2002**, *106*, 149.

(46) Sanderud, A.; private communication.

(47) Wetmore, S. D.; Boyd, R. J.; Eriksson, L. A. *J. Phys. Chem. B* **1998**, *102*, 7674. Ban, F.; Wetmore, S. D.; Boyd, R. J. *J. Phys. Chem. A* **1999**, *103*, 4303. Ban, F.; Gauld, J. W.; Boyd, R. J. *J. Phys. Chem. A* **2000**, *104*, 5080. Ban, F., Gauld J. W., Boyd R. J. *J. Phys. Chem. A* **2000**, *104*, 8583. Lahorte, P.; De Proft, F.; Vanhaelewyn, G.; Masschaele, B.; Cauwels, P.; Callens, F.; Geerlings, P.; Mondelaers, W. *J. Phys. Chem. A* **1999**, *103*, 6650. Lahorte, P.; De Proft, F.; Callens, F.; Geerlings, P.; Mondelaers, W. *J. Phys. Chem. A* **1999**, *103*, 11130.

(48) Fau, S.; Bartlett, R. J. *J. Phys. Chem. A* **2003**, *107*, 6648.